Autosomal dominant ApoA4 mutations present as tubulointerstitial kidney disease with medullary amyloidosis

see commentary on page 666

Tereza Kmochová[1,23], Kendrah O. Kidd[1,2,23], Andrew Orr[3,4,23], Aleš Hnízda[1], Hana Hartmannová[1], Kateřina Hodaňová[1], Petr Vyletal[1], Karolína Naušová[1], Vítězslav Brinsa[1], Helena Trešlová[1], Jana Sovová[1], Veronika Barešová[1], Klára Svojšová[1], Alena Vrbacká[1], Viktor Stránecký[1], Victoria C. Robins[2], Abbigail Taylor[2], Lauren Martin[2], Ana Rivas-Chavez[2], Riley Payne[2], Heidi A. Bleyer[2], Adrienne Williams[2], Helmut G. Rennke[5], Astrid Weins[5], Patrick J. Short[6], Varun Agrawal[7], Leroy J. Storsley[8], Sushrut S. Waikar[9], Ellen D. McPhail[10], Surendra Dasari[11], Nelson Leung[12], Tom Hewlett[13], Jake Yorke[4], Daniel Gaston[4], Laurette Geldenhuys[4], Mark Samuels[14,15,16], Adam P. Levine[17], Michael West[13], Helena Hůlková[1,18], Petr Pompach[19], Petr Novák[19], Richard B. Weinberg[20,21], Karen Bedard[22], Martina Živná[1,2], Jakub Sikora[1,18], Anthony J. Bleyer Sr[1,2] and Stanislav Kmoch[1,2]

[1]Research Unit for Rare Diseases, Department of Pediatrics and Inherited Metabolic Disorders, First Faculty of Medicine, Charles University, Prague, Czech Republic; [2]Section on Nephrology, Wake Forest University School of Medicine, Winston-Salem, North Carolina, USA; [3]Department of Ophthalmology and Visual Sciences, Dalhousie University, Halifax, Nova Scotia, Canada; [4]Department of Pathology, Faculty of Medicine, Dalhousie University, Halifax, Nova Scotia, Canada; [5]Pathology Department, Brigham and Women's Hospital, Harvard Medical School, Boston, Massachusetts, USA; [6]Sano Genetics Limited, London, UK; [7]Division of Nephrology and Hypertension, Larner College of Medicine, University of Vermont, Burlington, Vermont, USA; [8]Department of Medicine, University of Manitoba, Winnipeg, Manitoba, Canada; [9]Section of Nephrology, Boston University Chobanian and Avedisian School of Medicine, Boston, Massachusetts, USA; [10]Department of Laboratory Medicine and Pathology, Mayo Clinic, Rochester, Minnesota, USA; [11]Department of Quantitative Health Sciences, Mayo Clinic, Rochester, Minnesota, USA; [12]Division of Nephrology and Hypertension, Division of Hematology, Mayo Clinic, Rochester, Minnesota, USA; [13]Division of Nephrology, Department of Medicine, Faculty of Medicine, Dalhousie University, Halifax, Nova Scotia, Canada; [14]Department of Medicine Université de Montréal, Montreal, Quebec, Canada; [15]Department of Biochemistry, Université de Montréal, Montreal, Quebec, Canada; [16]Centre de Recherche du CHU Ste-Justine, Montreal, Quebec, Canada; [17]Research Department of Pathology, University College London, London, UK; [18]Institute of Pathology, First Faculty of Medicine, Charles University, Prague, Czech Republic; [19]Institute of Microbiology of the Czech Academy of Sciences, Vestec, Czech Republic; [20]Section on Gastroenterology, Department of Internal Medicine, Wake Forest University School of Medicine, Winston-Salem, North Carolina, USA; [21]Department of Physiology and Pharmacology, Wake Forest University School of Medicine, Winston-Salem, North Carolina, USA; and [22]Department of Pathology and Laboratory Medicine, Izaak Walton Killam Hospital, Halifax Nova Scotia, Canada

Sporadic cases of apolipoprotein A-IV medullary amyloidosis have been reported. Here we describe five families found to have autosomal dominant medullary amyloidosis due to two different pathogenic *APOA4* variants. A large family with autosomal dominant chronic kidney disease (CKD) and bland urinary sediment underwent whole genome sequencing with identification of a chr11:116692578 G>C (hg19) variant encoding the missense mutation p.L66V of the ApoA4 protein. We identified two other distantly related families from our registry with the same variant and two other distantly related families with a chr11:116693454 C>T (hg19) variant encoding the missense mutation p.D33N. Both mutations are unique to affected families, evolutionarily conserved and predicted to expand the amyloidogenic hotspot in the ApoA4 structure. Clinically affected individuals suffered from CKD with a bland urinary sediment and a mean age for kidney failure of 64.5 years. Genotyping identified 48 genetically affected individuals; 44 individuals had an estimated glomerular filtration rate (eGFR) under 60 ml/min/1.73 m^2, including all 25 individuals with kidney failure. Significantly, 11 of 14 genetically unaffected individuals had an eGFR over 60 ml/min/1.73 m^2. Fifteen genetically affected individuals presented with higher plasma ApoA4 concentrations. Kidney pathologic specimens from four individuals revealed amyloid deposits limited to the medulla, with the mutated ApoA4 identified by mass-spectrometry as the predominant amyloid constituent in all three available biopsies. Thus, ApoA4 mutations can cause autosomal dominant medullary amyloidosis, with marked amyloid deposition limited to the kidney medulla and presenting with autosomal dominant CKD

Correspondence: *Anthony J. Bleyer, Sr., Section on Nephrology, Wake Forest School of Medicine, One Medical Center Boulevard, Winston-Salem, North Carolina 27157, USA. E-mail: ableyer@wakehealth.edu*

[23]These authors contributed equally to the work.

Received 13 April 2023; revised 3 November 2023; accepted 10 November 2023; published online 12 December 2023

with a bland urinary sediment. Diagnosis relies on a careful family history, *APOA4* sequencing and pathologic studies.

Kidney International (2024) **105,** 799–811; https://doi.org/10.1016/j.kint.2023.11.021

KEYWORDS: AApoA-IV; ApoA4; autosomal dominant tubulointerstitial kidney disease; medullary amyloidosis

Copyright © 2023, International Society of Nephrology. Published by Elsevier Inc. All rights reserved.

Lay Summary

In this article, we identify changes ("mutations") in the gene *APOA4* as a cause of inherited kidney disease. Apolipoprotein A-IV (ApoA4) is a protein that transports fat molecules from the intestines via the bloodstream to cells throughout the body. After the fat molecules are removed from ApoA4, it is filtered by the kidney and reabsorbed back into the bloodstream. In this study of 5 families, we identified 1 mutation in 3 families, and another mutation in 2 families. In both cases, the mutations affect the ApoA4 structure and result in deposition of abnormal ApoA4 in the middle (medulla) of the kidney. This abnormal protein deposition leads to slowly progressive kidney failure, often leading to the need for dialysis later in life. The article is important because it identifies a new form of inherited kidney disease. Now patients can be tested for the disease, and scientists can start to develop treatments.

Genetic causes increasingly are being identified in families presenting with chronic kidney disease (CKD) with a bland urinary sediment and autosomal dominant inheritance.[1] The most common causes are autosomal dominant tubulointerstitial kidney disease (ADTKD) due to *UMOD*[2] or *MUC1*[3] mutations, each accounting for approximately 0.3% of cases of kidney failure resulting in the need for dialysis or kidney transplantation in the US.[4–6] Other families also have an ADTKD-like presentation (autosomal dominant CKD with a bland urinary sediment) in which the genetic cause of kidney disease has not been identified.

In this investigation, we identify 2 different variants in the *APOA4* gene encoding human apolipoprotein A-IV (ApoA4) in 48 individuals from 5 families with an ADTKD-like presentation. ApoA4 is a 46-kDa apolipoprotein that is synthesized in intestinal enterocytes in response to dietary fat absorption[7] and incorporated onto the surface of nascent chylomicrons. Once chylomicrons enter the circulation, ApoA4 dissociates from the chylomicron and circulates in a manner loosely associated with high-density lipoproteins[8] as a lipid-free glycoprotein with a molecular weight of 46 kD[9] and as a stable homodimer with a molecular weight of 92 kD.[10] The kidney plays a major role in ApoA4 metabolism. Monomeric ApoA4 is small enough to undergo glomerular filtration,[11] with subsequent reabsorption and degradation in proximal and distal tubules.[11]

ApoA4 has been found in rare cases to be the primary constituent of amyloid deposits occurring exclusively in the kidney medulla, with 13 cases of sporadic AApoAIV (amyloid-ApoAIV) medullary amyloidosis having been described in the literature[12–14] or presented as an abstract (Sheikh SN, Li T, Kunjal RA. Apolipoprotein A-IV amyloidosis: an unusual cause of renal amyloidosis and CKD. Presented at: American Society of Nephrology Kidney Week. October 23–25, 2018; San Diego, CA. TH-PO523). In all cases, AApoAIV deposition was limited to the kidney medulla. Of the 13 cases, 12 presented with CKD and a bland urinary sediment with minimal proteinuria; 1 presented with advanced CKD and 5.8 g/d of urinary protein.[13]

As in reports of sporadic AApoaIV medullary amyloidosis, pathologic examination of kidney tissue from 4 genetically affected individuals from our investigation revealed isolated medullary amyloid deposition, with mass-spectrometric analysis of tissue available from 3 patients revealing mutated ApoA4 protein as the predominant constituent. Thus, in this investigation, we report for the first time cases of *APOA4* variants causing autosomal dominant medullary amyloidosis and a presentation of CKD with a bland urinary sediment.

METHODS

This investigation was approved by the institutional review boards of Wake Forest School of Medicine (Winston-Salem, NC, United States), Charles University (Prague, Czech Republic), and Nova Scotia Health (Halifax, Nova Scotia, Canada).

The Wake Forest Rare Inherited Kidney Disease Registry includes DNA from 429 families with autosomal dominant CKD with a bland urinary sediment.[15] Participants with autosomal dominant CKD with a bland urinary sediment who are not found to have a known causative mutation then undergo whole-exome or whole-genome analysis with systematic reanalysis for unsolved cases.

Genetic evaluation

Genomic DNA of all available individuals was extracted from whole blood or saliva. Sanger sequencing, whole-exome and whole-genome sequencing, data analysis, variant prioritization, and targeted genotyping were performed as described.[16] Obligate heterozygotes were included in the analysis only if age of initiation of dialysis or transplantation was available.

In silico analysis

Mutations were mapped into the ApoA4 crystal structure[17] or a theoretical model of the dimeric full-length protein generated by AlphaFold2-multimer available via ColabFold.[18] Structural models were visualized with PyMOL viewer (Schrödinger Inc.) and UCSF ChimeraX (DeLano Scientific). Amyloidogenic regions in ApoA4 were identified using MetAmyl[19] and AmyloPred2.[20]

Amyloid proteomic analysis

The proteomic content of microdissected amyloid deposits from pathologic specimens was analyzed as previously described.[13]

Histopathologic, immunohistochemical, immunofluorescent, and ultrastructural electron microscopic analyses of kidney biopsies

Standard staining was performed as previously described.[6] See the Supplementary Methods for information on the specific antibodies that were used.

Immunoblot analysis of ApoA4 in plasma

Plasma samples were separated by non-denaturing polyacrylamide gel electrophoresis, and ApoA4 was immunodetected as previously described.[21] For immunodetection, mouse anti-human ApoA4 antibody (G-8) (sc-374543, Santa Cruz) was used. Immunoaffinity enrichment of plasma ApoA4 with mass spectrometry analysis typing was performed as previously described,[22] with details provided in the Supplementary Methods.

Statistical analysis

Standard statistical analyses were performed with SAS (SAS Institute). Estimated glomerular filtration rate (eGFR) was calculated with the Chronic Kidney Disease Epidemiology Collaboration (CKD-EPI) equation.[23] To assess the differences in plasma ApoA4 levels between those with *APOA4* risk genotypes and those unaffected, a mixed-effects model with compound-symmetry covariance structure was applied to account for the correlation between related individuals.

RESULTS

The index case III.12 from Family 1 (Figure 1) is a male patient who presented at age 54 years with CKD of unknown cause. In his early 40s, the patient was diagnosed with hypertension, gout, and hypercholesterolemia. The patient was placed on atorvastatin, 60 mg daily, for hyperlipidemia. The patient never experienced a cardiovascular event. The patient's father died in his 80s without CKD, and his mother's eGFR was 55 ml/min per 1.73 m^2 at age 90 years. A sister of the proband (III.9) underwent kidney transplantation at age 68 years, and a brother's (III.11) eGFR was 19 ml/min per 1.73 m^2 at age 57 years. Cardiovascular disease occurred only after age 50 years in family members with and without CKD. Physical examination was unremarkable. The patient's urinalysis was bland, with pH 5.5 and no urinary protein. The eGFR was 44 ml/min per 1.73 m^2. A fasting lipid panel of the patient at age 52 years while on atorvastatin revealed a total cholesterol of 193 mg/dl (normal range [nr] 25–200 mg/dl), triglycerides 176 mg/dl (nr <150 mg/dl), high-density lipoprotein cholesterol 49.6 mg/dl (nr 35–135 mg/dl), and low-density lipoprotein cholesterol 108 mg/dl (nr <130 mg/dl). On kidney imaging at age 55 years, the right kidney was 11.3 cm with 2 cortical cysts, and the left kidney was 12.7 cm with a simple cyst. A kidney biopsy at age 54 years (Table 1) revealed advanced chronic changes in all compartments of the kidney parenchyma, with about 60% globally sclerotic glomeruli, tubular atrophy, interstitial fibrosis, and severe vascular sclerotic changes. No amyloid deposition was noted. CKD progressed to initiation of

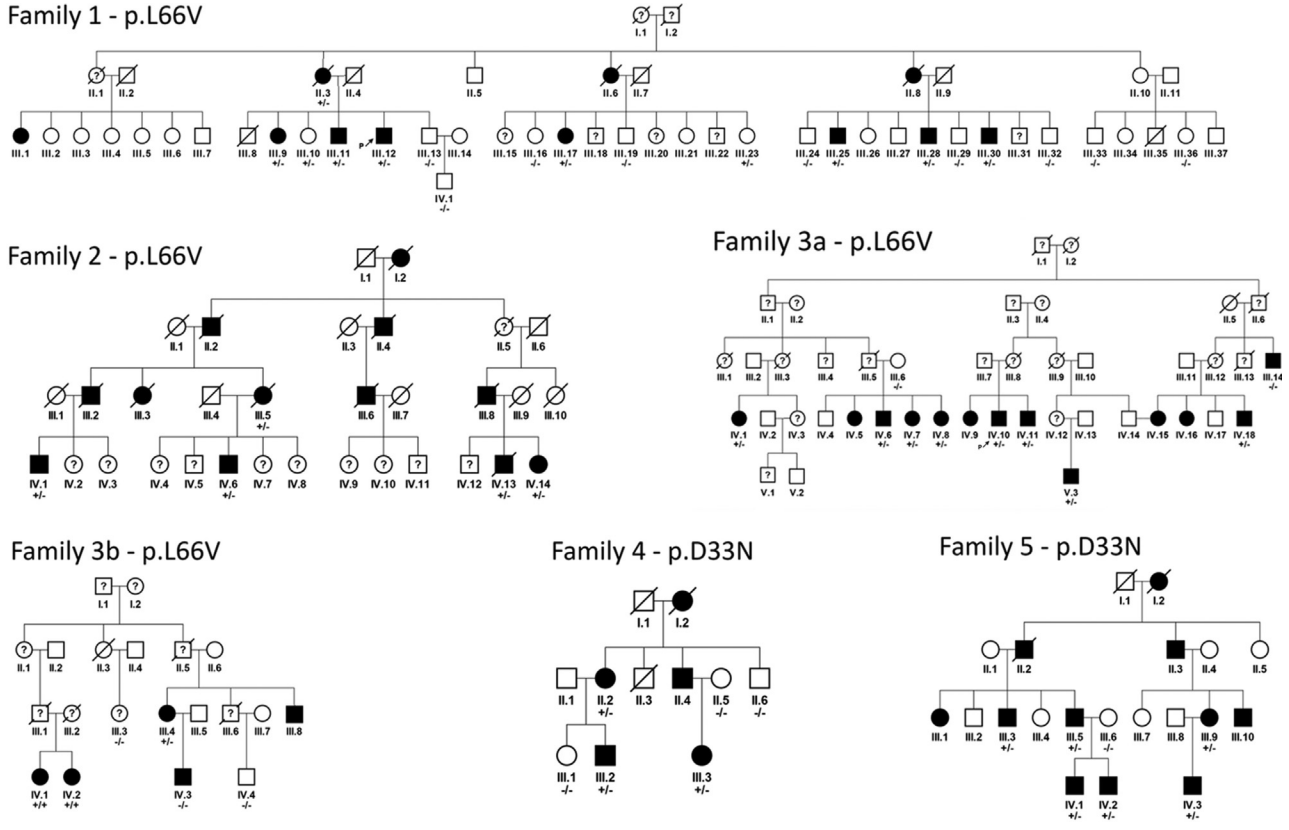

Figure 1 | Family pedigrees. Filled-in shapes denote chronic kidney disease, and unshaded shapes denote normal kidney function. A question mark (?) denotes lack of information on clinical status. A plus sign (+) indicates the presence of the p.L66V or p.D33N *APOA4* variant, and a minus sign (–) indicates the presence of the wild-type *APOA4* variant in a genotyped individual. Two plus signs (+/+) indicates the presence of 2 p.L66V *APOA4* variants. Unfortunately, no clinical and/or laboratory data were available for the parents of the 2 homozygotes in Family 3b, IV.1 and IV.2. Additional pedigree branches of Family 3 are presented in Supplementary Figure S1.

Table 1 | Pathologic findings

Individual and mutation	eGFR at time of biopsy, ml/min per 1.73 m^2	Bx type	Glomeruli	Tubule changes	Tubulointerstitium	Microvascular changes	EM	Medulla	CR/ApoA4 staining
Family 1, III.12 p.L66V	54	Core	Glomerulo-sclerosis. Double contours of GBMs	TA	IF	Severe vascular sclerotic changes	The displaced glomerular endothelium has developed a newly formed thin layer of basement membrane material	Not present	CR staining and ApoA4 staining revealed no interstitial amyloid, amyloid casts, or abnormal cytoplasmic ApoA4 signal.
Family 1, III.12 p.L66V	10	Nx	Global glomerulo-sclerosis. No double contours seen.	TA	Marked IF	Moderate sclerosis	Fibrils approximately 8.5 nm in diameter in criss-crossing bundles (Figure 5b)	Extensive deposition of amorphous eosinophilic material	Strongly congophilic with apple-green birefringence limited to inner medulla
Family 2, IV.1 p.L66V	46	Core	Glomerulosclerosis	Basement membrane thickening and atrophy	Mild chronic inflammatory cell infiltrate with fibrosis	Vessels are mildly thickened and demonstrate hyaline changes in the vessel walls	Fine non-branching fibrils arranged in criss-crossing bundles, confirming the presence of amyloid	Advanced involvement of the tubules and interstitium by a hyaline, "brittle" material, which is PAS-negative.	CR stains demonstrate positive staining in the hyaline areas, which appear under polarization as apple-green birefringence
Family 2 V.3 p.L66V	53	Core	Glomerulo-sclerosis. Bowman's capsule is thickened and lamellated.	Atrophic tubules. TBM shows areas of lamellation.	Scattered chronic inflammation. Increased collagen.	Focal hyalinosis	No EDD	No medulla present	CR staining and ApoA4 staining revealed no interstitial amyloid, amyloid casts, or abnormal cytoplasmic ApoA4 signal.
Family 4 III.2 p.D33N	73	Core	Glomerulo-sclerosis. Wrinkling of the GBM	Mild patchy TA. No tubulitis	Patchy interstitial mononuclear inflammatory cell infiltrate.	Unremarkable	Unavailable	No medulla present	CR staining and ApoA4 staining revealed no interstitial amyloid, amyloid casts, or abnormal cytoplasmic ApoA4 signal.
Family 4, III.3 p.D33N	39	Core	Glomerular hypertrophy. Focal global glomerulosclerosis, moderate	Focal TBM multilamellation. Diffuse TA	Mild chronic inflammatory infiltrate of mononuclear leukocytes	Mild to moderate ARS	No comment	No medulla present	CR staining and ApoA4 staining revealed no interstitial amyloid, amyloid casts, or abnormal cytoplasmic ApoA4 signal.
Family 3a, III.14 p.L66V	On dialysis	Nx	Extensive glomerulosclerosis. Basement membrane wrinkling	Marked TA and IF	Moderate patchy interstitial lymphoid infiltrate	Marked arterial and ARS	Unavailable	Amyloid deposition. Focal calcification and ossification	Positive CR staining—salmon pink with apple-green birefringence
Family 3a, IV.10 p.L66V	61	Core	Medulla only	Unremarkable medullary tubules	Unremarkable medullary tubules	No arteries identified	Unavailable, no glomeruli	Amyloid deposition	Positive CR staining—salmon pink with apple-green birefringence

ARS, arteriosclerosis; Bx, biopsy; CR, Congo Red; EDD, electron-dense deposit; eGFR, estimated glomerular filtration rate; EM, electron microscopy; GBM, glomerular basement membrane; IF, interstitial fibrosis; Nx, nephrectomy; PAS, periodic acid–Schiff; TA, tubular atrophy; TBM, tubular basement membrane.

dialysis at age 66 years. Family history revealed numerous family members who were affected similarly clinically, with an autosomal dominant inheritance pattern (Figure 1).

Genetic analysis

Upon negative results of *UMOD* and *MUC1* genotyping, whole-genome sequencing was performed in 5 clinically affected individuals from family 1 (III.9, III.11, III.12, III.25, and III.30). A search for shared genetic material identified only one ∼15–megabase pair (Mbp)–sized genomic region on chromosome 11 (chr11: 110012896-124998347), with only one relevant candidate variant—chr11:116692578 G>C (hg19)—encoding for a missense mutation in *APOA4* (NM_000482.4): c.196C>G (p.L66V). No other rare protein coding or conserved regulatory variants were shared by affected individuals elsewhere in their genomes. Using Sanger sequencing and segregation analysis, we genotyped 19 individuals from Family 1. Of 11 genetically affected individuals (10 genotyped and one obligate heterozygote), 9 had CKD, with 2 female members (III.10 and III.23) being as yet clinically unaffected (eGFR 100 ml/min per 1.73 m^2 at age 55 years, and eGFR 86 ml/min per 1.73 m^2 at age 54 years, respectively). Of 9 genetically unaffected individuals, the lowest eGFR was 59 ml/min per 1.73 m^2 at age 69 years (Figure 2a).

A search for rare *APOA4* variants from our internal whole-genome sequencing/whole-exome sequencing database revealed the following results:

(i) The same chr11:116692578 G>C (p.L66V) variant was present in 7 clinically affected individuals (5 genotyped and 2 obligate heterozygotes) from Family 2 (Figure 1) and in the proband IV.10 from Family 3a, who was later found to be part of a large kindred from a rural area in Nova Scotia, Canada, where an unusually high incidence of CKD had been noted by researchers from Dalhousie University. The different branches of this kindred are displayed as Families 3a and 3b in Figure 1, and Families 3c–f in Supplementary Figure S1. High-density single-nucleotide polymorphism genotyping was carried out on 13 affected members of the Nova Scotia pedigrees and an analysis was performed using the combinatorial conflicting homozygosity (CCH) method, an efficient nonparametric technique that is well suited to identifying haplotypes shared identical-by-descent in founder populations.[24] This revealed a 2.8-Mbp region at chr11: 116369171-119235404 shared by all 13 individuals. Taken together with the mapping described above, this narrowed the critical interval to an ∼1 Mbp–sized region at chr11: 116369171-117651600, still containing *APOA4*. The p.L66V variant segregated with affected status. In further analysis, the p.L66V variant was identified in 17 individuals, all of whom were clinically affected. Two clinically affected individuals were genetically unaffected: III.14 from Family 3a, with an eGFR of 12 ml/min per 1.73 m^2 at age 94 years, and IV.3 from Family 3b, with an eGFR of 30 ml/min per 1.73 m^2 at age 77 years (Figure 2a). Two individuals homozygous for the p.L66V variant (IV.1 and IV.2 from Family 3b) had clinical findings similar to those for heterozygous individuals (Figure 2a).

(ii) The ch11:116693454 C>T (hg19) variant encoding for another missense mutation in *APOA4* (NM_000482.4): c.97G>A (p.D33N) was identified in 5 clinically affected individuals (3 genotyped and 2 obligate heterozygotes)

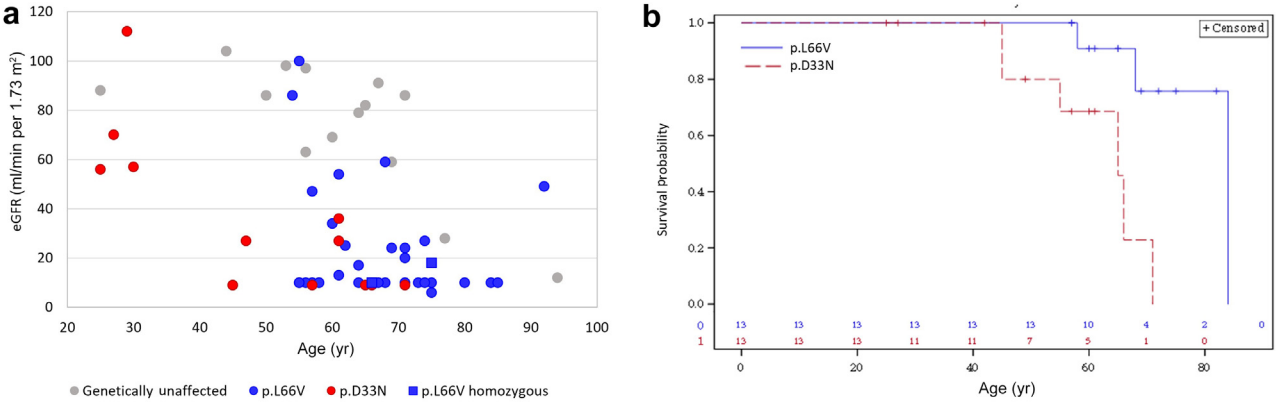

Figure 2 | Kidney function in affected individuals. (**a**) The most recent estimated glomerular filtration rate (eGFR, ml/min per 1.73 m^2) versus age in individuals affected with the ApoA4 p.D33N mutation, the ApoA4 p.L66V mutation, and genetically unaffected individuals from the 5 families. Individuals on dialysis/transplanted were assigned an eGFR of 10 ml/min per 1.73 m^2 at the time of first initiation of dialysis or transplantation. All genetically unaffected individuals had an eGFR ≥ 59 ml/min per 1.73 m^2. Individuals affected with the p.L66V mutation started dialysis or underwent kidney transplantation at a later age and had milder eGFR decline than individuals with the p.D33N mutation. Two individuals affected with the p.L66V variant had an eGFR > 80 ml/min per 1.73 m^2 at age >50 years, and one genetically affected individual with the p.L66V variant had an eGFR of 58 ml/min per 1.73 m^2 at age 91 years. The genetically unaffected individuals had normal kidney function, except for 3 individuals—one patient had an eGFR of 59 ml/min per 1.73 m^2 at age 69 years, another had an eGFR of 30 ml/min per 1.73 m^2 at age 77 years, and another had an eGFR of 12 ml/min per 1.73 m^2 at age 94 years. (**b**) Survival curve to first initiation of dialysis or kidney transplantation according to mutation and sex. Events included start of dialysis, date of preemptive kidney transplantation, and date of death from uremia. Censoring occurred at end of follow-up or at death from non-kidney causes.

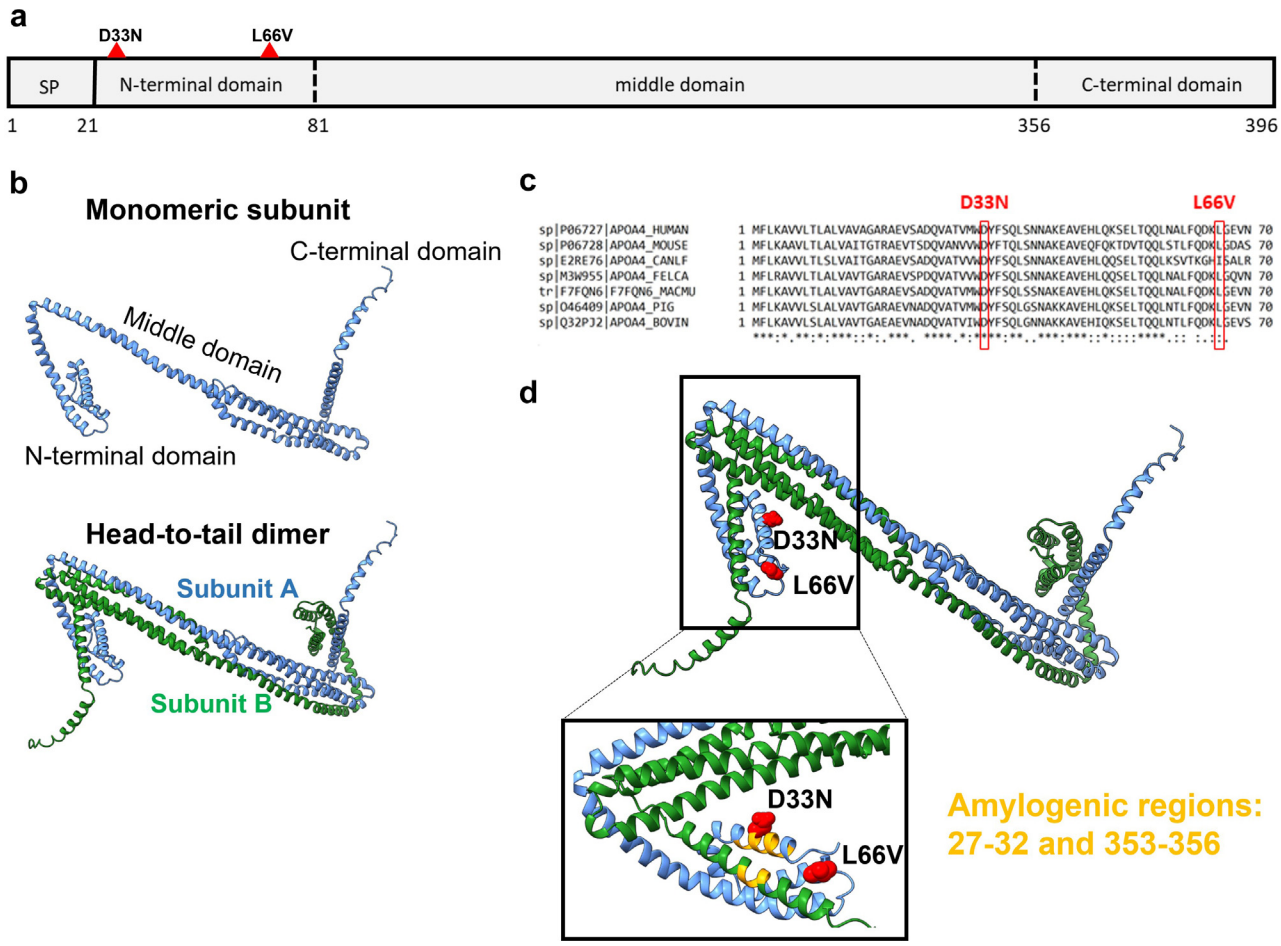

Figure 3 | Structural impact of ApoA4 mutations. (**a**) Domain architecture of ApoA4, with the signal peptide (SP) spanning amino acid (aa) residues 1–20 and the mature protein (aa 21–396) composed of the N-terminal, middle, and C-terminal domains. Red triangles show the locations of the identified mutations. (**b**) Theoretical model of dimeric ApoA4 molecule generated by AlphaFold2-Multimer. Upper and lower panels illustrate the domain architectures of the ApoA4 monomer and the tail-to-head oriented dimer. Each ApoA4 subunit is depicted in a different color. (**c**) Homology of the mutant and wild-type ApoA4 N-terminal domain with those of higher mammals shows a high degree of sequence conservation at the mutated residues. (**d**) Localization of mutations in the structural model of mature ApoA4 is highlighted by red spheres in a single subunit of dimeric assembly. Amyloidogenic regions predicted by MetAmyl[19] and AmyloPred2[20] software are detailed in orange.

from Family 4, and 8 clinically affected individuals (6 genotyped and 2 obligate heterozygotes) from Family 5.

Thus, the identified *APOA4* variants segregated in an autosomal dominant pattern. In summary, 44 of 48 genetically affected individuals had an eGFR <60 ml/min per 1.73 m^2, and 11 of 14 genetically unaffected individuals had an eGFR >60 ml/min per 1.73 m^2 (Figure 2a; $P < 0.0001$). All 25 of the 25 individuals who developed the need for dialysis or kidney transplantation were genetically affected.

Examination of haplotypes across the *APOA4* genomic region showed that probands carrying the same variant shared identical mutation-carrying chromosomal segments from a common ancestor, indicating that affected families are highly likely to be related. Both genetic variants reside on the "wild-type" ApoA4-1 isoform in all families.[25] Neither of these variants have been reported in The Genome Aggregation Database (gnomAD), and both affect an evolutionarily conserved amino acid located in the ApoA4 N-terminal amyloidogenic domain (Figure 3; Supplementary Figure S2).[26]

Clinical findings in the 5 families

Urinary protein/creatinine measurements (Supplementary Figure S3) were <300 mg/g in 10 of 11 genetically affected individuals, with one individual with an eGFR of 52 ml/min per 1.73 m^2 having a measurement of 867 mg/g, consistent with proteinuria in CKD due to reduced nephron mass.[27] In 8 patients with urinary albumin/creatinine measurements, 6 were <250 mg/g, with one patient with an eGFR of 25 ml/min per 1.73 m^2 having a measurement of 949 mg/g, and another with an eGFR of 30 ml/min per 1.73 m^2 having a measurement of 720 mg/g. Kidney function in genetically unaffected versus genetically affected individuals is shown in Figure 2a. Two individuals are affected with the p.L66V variant, with an eGFR > 80 ml/min per 1.73 m^2 at age >50 years, and one individual is genetically affected with the p.L66V variant, with an eGFR of 58 ml/min per 1.73 m^2 at age 91 years. Two patients homozygous for the p.L66V mutation had rates of eGFR decline similar to those of heterozygous individuals (Figure 2a). Kidney imaging was consistent with

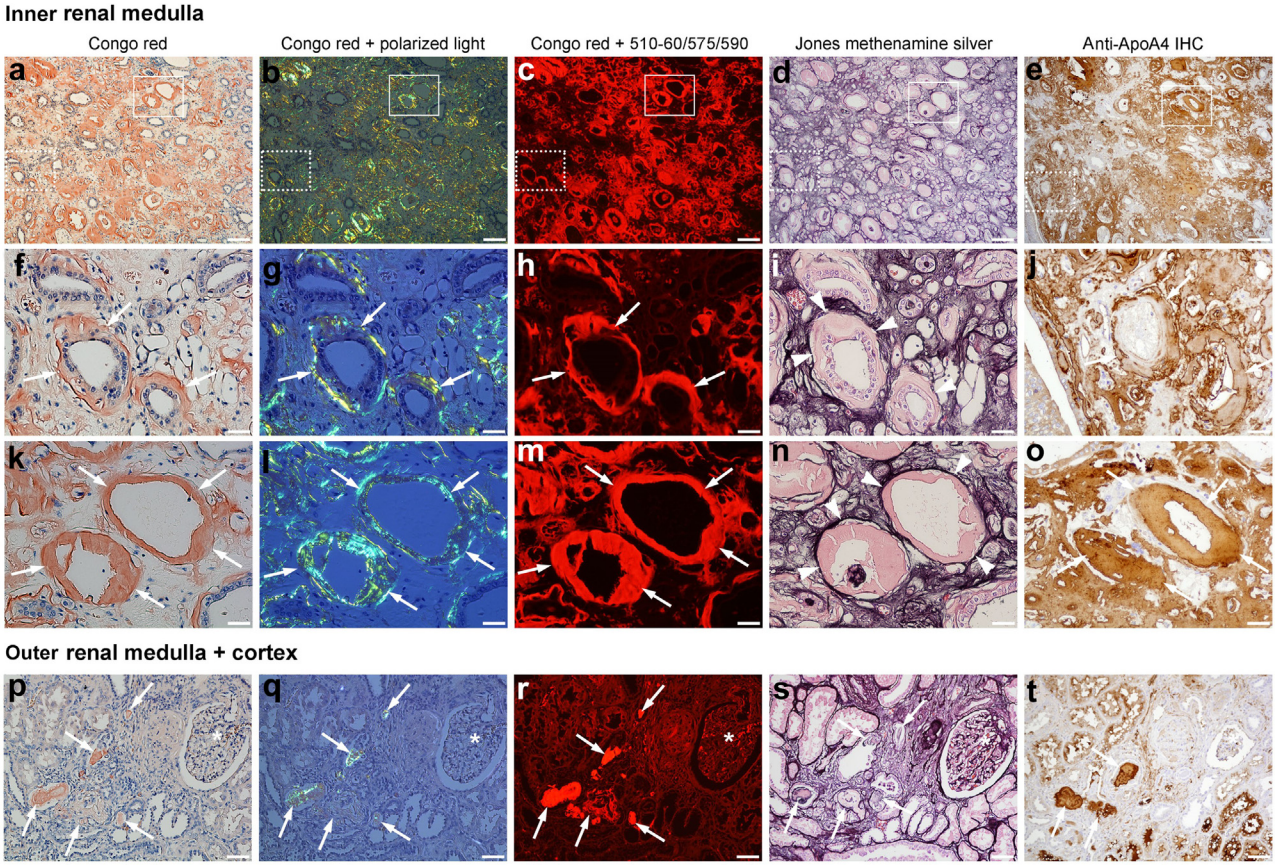

Figure 4 | Light microscopy, including Congo-red staining, of the cortex and medulla in the nephrectomy specimen from an affected individual. Three serial sections were stained with (**a–c,f–h,k–m,p–r**), Congo red (**d,i,n,s**) Jones methenamine silver, and (**e,j,o,t**) anti-ApoA4 Ab. Dashed white rectangles in (**c–e**) correspond to areas shown in (**f–j**), respectively. White solid rectangles in (**a–e**) correspond to areas shown in (**k–o**), respectively. Identical fields of view in Congo-red staining are shown under (**a,f,k,p**) normal transmitted light, (**b,g,l,q**) polarized light, and (**c,h,m,r**) epifluorescence (for example, BP 510-560/DM575/LP 590). Amyloid accumulation can be seen in the inner medulla (kidney papilla). Amyloid localizes interstitially but also under the epithelia of collecting ducts. (**f–h,i**) Subepithelial amyloid accumulation is highlighted by white arrows (white arrowheads mark the epithelial basal membranes). (**k–n**) Some of the collecting ducts are completely lined by amyloid deposits and lack surface epithelium. (**n**) Residual epithelial basal membranes are highlighted by white arrowheads. (**e,j,o**) Amyloid deposits (variably) stain with anti-ApoA4 Ab, compared to corresponding serial sections stained by (**c,h,m**) Congo red and (**d,i,n**) Jones methenamine silver. (**p–t**) Numerous amyloid tubular casts can be found in outer kidney medulla and cortex (highlighted by white arrows. Similar intratubular casts can be also found in inner medulla collecting ducts (not shown). Asterisks highlight one glomerulus. Bar = (**a–e**) 200 μm; (**f–o**) 50 μm; and (**p–t**) 100 μm. IHC, immunohistochemical. To optimize viewing of this image, please see the online version of this article at www.kidney-international.org.

CKD. Supplementary Figure S4A shows a similar figure by sex and pathogenic variant, including genetically unaffected individuals, obligate carriers, and clinically affected individuals (CKD stage ≥3b) in whom DNA could not be obtained. The mean age of initiation of dialysis or kidney transplantation was 58.2 ± 11.1 years (range: 45–71 years) for individuals with the p.D33N variant, and 66.7 ± 10.2 years (range: 55–85 years) for individuals with the p.L66V variant ($P = 0.1$). To compare disease severity between the p.D33N and the p.L66V variants, survival curves (Figure 2b; Supplementary Figure S4B) and a Cox proportional hazards model were created with the outcome variable being age of first initiation of dialysis or kidney transplantation, and with independent variables including sex and mutation. In univariate models, the hazard ratio for the p.D33N genotype was 7.8 (95% confidence interval [CI] 1.30–46.97, $P = 0.01$), and for male sex, it was 4.51 (95% CI 0.75–27.27), $P = 0.07$. The best-fit model included only genotype.

In 22 genetically affected individuals with available data, 4 suffered cardiac events at age 55, 58, 65, and 70 years. Eight of 24 affected individuals were receiving lipid-lowering agents. Lipid profiles were available in 5 genetically affected individuals who were not receiving statins. The mean cholesterol level was 199 ± 49 mg/dl; high-density lipoprotein cholesterol was 62.4 ± 20.1 mg/dl; very-low-density lipoprotein cholesterol was 13 ± 1.4 mg/dl (nr 2–30 mg/dl); and low-density lipoprotein cholesterol was 118 ± 50 mg/dl.

To identify other potential clinical manifestations of amyloidosis, a chart review and/or interview revealed normal serum alkaline phosphatase and normal serum albumin levels in 9 of 9 available patients. In surveying 14 genetically affected

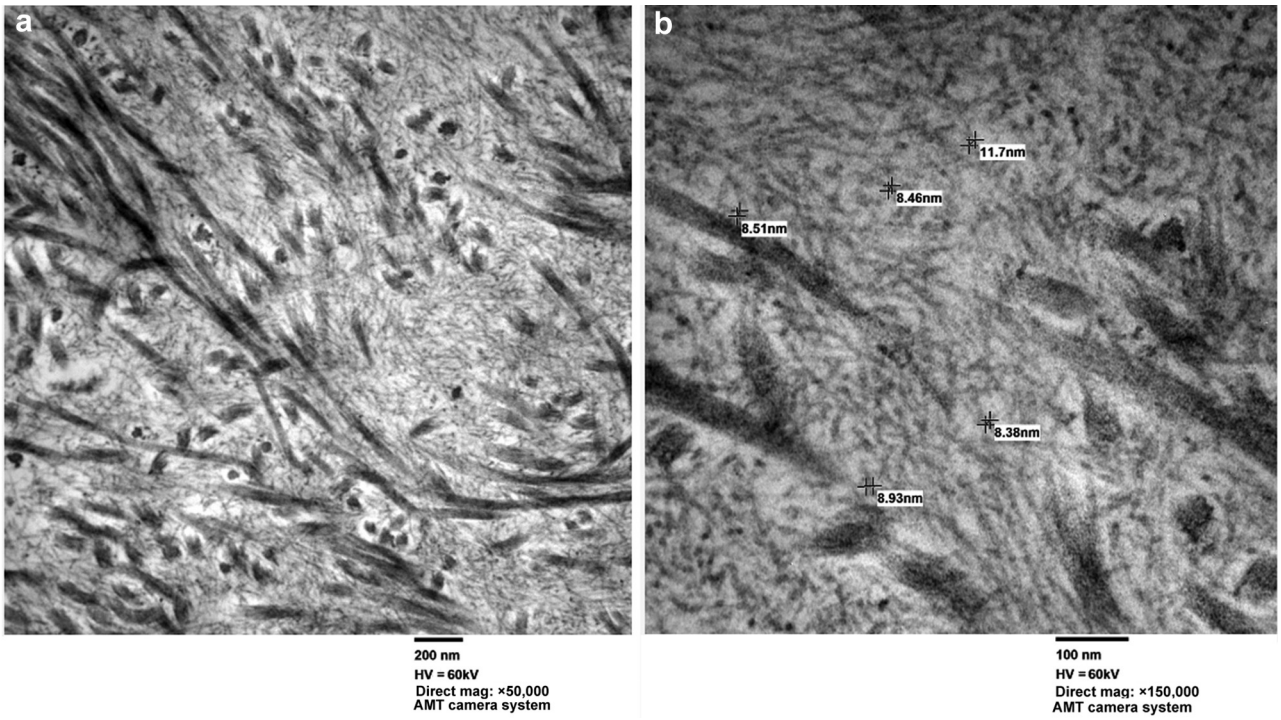

Figure 5 | Electron microscopy of amyloid fibrils at (a) x50,000 and (b) x150,000 demonstrates a crisscrossing pattern with a fibril diameter of approximately 8.5 nm.

individuals, 1 of 14 (Family 5, III.3) had heart failure (diagnosed with cardiac transthyretin amyloidosis), and 0 of 14 had hepatomegaly or chronic problems with diarrhea or constipation. Three of 14 patients, all aged >60 years and with advanced CKD, reported increased susceptibility to bruising that had not required physician referral. Besides the cardiac biopsy showing transthyretin amyloidosis, 0 of 14 patients underwent biopsies of the intestine, heart, liver, or other organs, except for the kidney.

Histopathologic, immunohistochemical, and proteomic analyses

Pathologic findings from 8 kidney specimens are presented in Table 1. Pathology consistently showed secondary global glomerulosclerosis and tubulointerstitial fibrosis. Four of 8 pathologic specimens contained inner medulla, with all showing hyaline material restricted to the medulla (Figure 4). Of the 4 cases with inner medulla, 2 were nephrectomy samples (III.12 from Family 1 and III.14 from Family 3a), 1 was a core biopsy with limited material (IV.10 from Family 3a), and in 1 case (IV.1 from Family 2), only a biopsy report was available. In 3 of the 4 cases, hyaline deposits consistent with amyloid deposition were noted only in secondary analysis after the mutation had been identified. Congo-red staining revealed apple-green birefringence under polarized light (Table 1; Figure 4; Supplementary Figure S5) in all 4 cases. For III.12, electron microscopy of the medulla showed fine nonbranching fibrils approximately 8.5 nm in diameter arranged in crisscrossed bundles (Figure 5a). Similar findings appeared in the electron microscopy report from IV.1. Four biopsies containing only kidney cortex showed no pathologic staining with Congo red or ApoA4 (Table 1).

Patient III.12 underwent nephrectomy at age 67 years after a genetic diagnosis had been made, allowing detailed immunohistologic examination of both the cortex and medulla. Examination of the kidney cortex revealed tubular atrophy, and interstitial fibrosis with advanced global glomerulosclerosis (Figure 4). In the inner medulla (kidney papilla), extensive amyloid accumulation was present in the interstitium and under the epithelia of collecting ducts. Some of the collecting ducts were completely lined by amyloid and lacked surface epithelium. Numerous amyloid intratubular casts were found in the medulla and cortex. We categorized the tubules containing amyloid casts as collecting ducts based on their light microscopic morphology, localization, and distribution in the tissue. No cytoplasmic amyloid deposits in the tubular epithelia were detected anywhere in the tissue.

Aside from the normal granular ApoA4 signal in epithelia of proximal tubules, we identified an abnormal and intense diffuse ApoA4 signal in the cytoplasm of epithelia of a fraction of cortical and medullary tubules that were uromodulin-negative. Lack of the granular cytoplasmic ApoA4 signal, together with absence of uromodulin in these abnormally ApoA4-stained epithelia, suggested that they were likely collecting ducts. The majority of the interstitial amyloid deposits stained positive with ApoA4 antibody (Figure 4; Supplementary Figures S5, S6, and S7).

Congo red–positive amyloid deposits were laser-microdissected and subjected to proteomics analysis

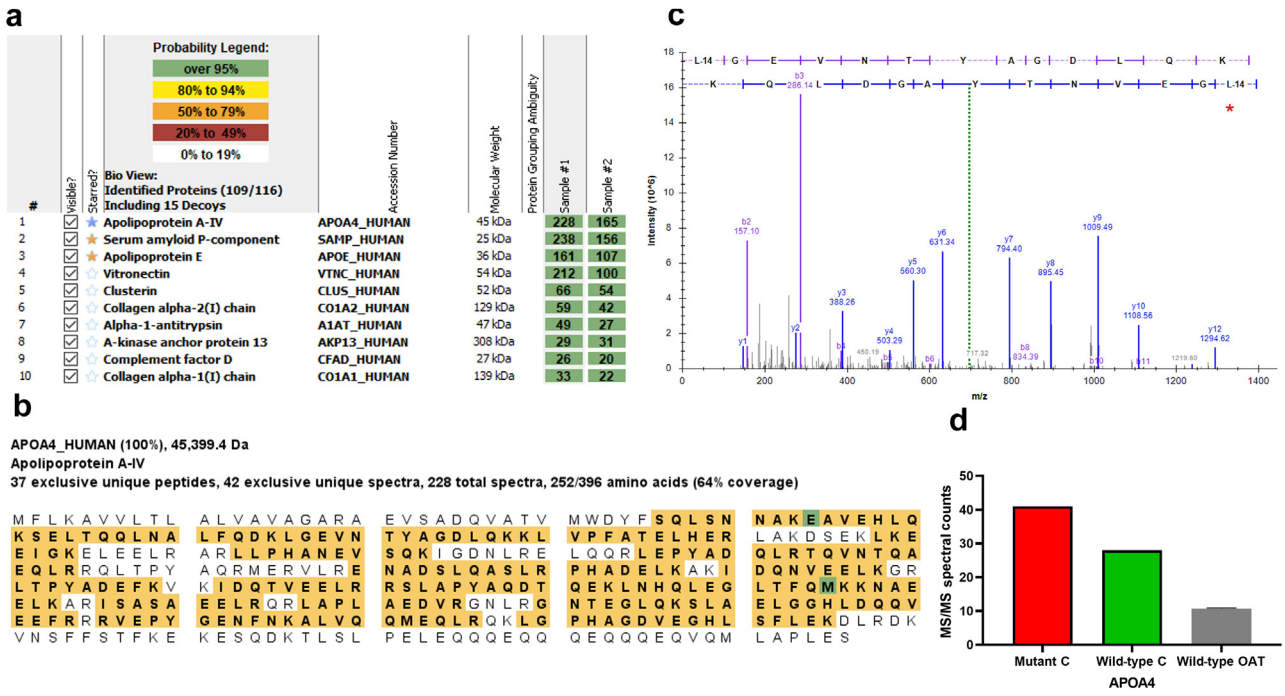

Figure 6 | Proteomic identification of mutant ApoA4 in amyloid deposits. Congo red–positive amyloid deposits were laser microdissected and subjected to proteomics analysis. Two independent microdissections were performed, and each was analyzed separately. (**a**) Protein identification profile showing top 10 proteins detected in the patient amyloid deposits. The yellow star highlights universal amyloid signature proteins. The blue star represents amyloidogenic protein in the patient's amyloid deposits. Values in green boxes are the total number of tandem mass spectrometry (MS/MS) spectra matching to the corresponding protein in each sample. (**b**) Sequence coverage of ApoA4 protein detected in the patient. Bold letters on yellow highlighted background represent the portions of protein detected in the patient. (**c**) The MS/MS spectrum corresponding to the p.L66V is shown. The red asterisk shows the mutated amino acid. (**d**) Mutant-C and wild type-C represent the total number of MS/MS spectra matching to the p.L66V peptide and the corresponding wild-type ApoA4 peptide present in the patient's amyloid deposit. Wild type-OAT (other amyloid type) represents the average total number of MS/MS spectra matching to the same wild-type ApoA4 peptide in non-AApoAIV kidney amyloidosis cases (N = 905). The p.L66V mutant peptide was not detected in these N = 905 non-AApoAIV kidney amyloidosis cases.

(Figure 6). Approximately 100 proteins were in the deposit, with the mutant ApoA4 being the most abundant amyloidogenic protein. Approximately 350 spectral counts of ApoA4 were present, similar to cases of sporadic AApoAIV amyloidosis. The ratio of the ApoA4 peptide containing the mutated p.L66V residue to wild-type ApoA4 was 1.46 to 1.

The nephrectomy sample from III.14 showed extensive amyloid deposition (see Supplementary Figure S5) and positive ApoA4 immunohistochemical staining. The tissue was from a patient with advanced kidney failure on dialysis, precluding detailed analysis of ApoA4 deposition similar to that of the specimen from III.12. Laser microdissection and proteomic analysis revealed approximately 121 proteins in the deposit, with the mutant ApoA4 being the most abundant amyloidogenic protein. Approximately 137 spectral counts of ApoA4 were present, similar to cases of sporadic AApoAIV amyloidosis. The ratio of the ApoA4 peptide containing the mutated p.L66V residue to wild-type ApoA4 was approximately 2 to 1. The needle biopsy from IV.10 revealed amyloid deposition in the medulla, but no tissue remained for ApoA4 immunostaining. Laser microdissection and proteomic analysis revealed approximately 335 spectral counts of ApoA4. The ratio of the ApoA4 peptide containing the mutated p.L66V residue to wild-type ApoA4 was approximately 2 to 1.

Skin biopsy samples were available from two family 1 members, III.12 and III.28. Amyloid deposits were not detected in these samples using Congo-red staining (not shown).

Plasma ApoA4 analysis

Plasma ApoA4 was immunodetected in 15 individuals with the ApoA4 variants (7 with the p.D33N variant, and 8 with the p.L66V variant), and 49 controls (6 genetically unaffected family members, 6 with *MUC1* mutations, 12 with *UMOD* mutations, and 24 population controls; Figure 7a and b). Plasma total ApoA4 levels were increased for patients with *ApoA4* mutations versus controls (840 ± 226 vs. 515 ± 188 ng, $P = 0.0001$), as well as plasma monomeric ApoA4 (578 ± 151 vs. 406 ± 110 ng, $P = 0.0001$) and plasma dimeric ApoA4 (262 ± 83 vs. 109 ± 132 ng, $P = 0.06$). Immunoaffinity enrichment with mass spectrometry analysis revealed that the ratio of mutated ApoA4 and wild-type ApoA4 was approximately 1 to 1 (Supplementary Figure S8).

In silico analysis

ApoA4 consists of a middle domain comprised of 13 proline-punctuated amphipathic helices (residues 84–355) and globular and/or coiled domains at the N- and C-terminus

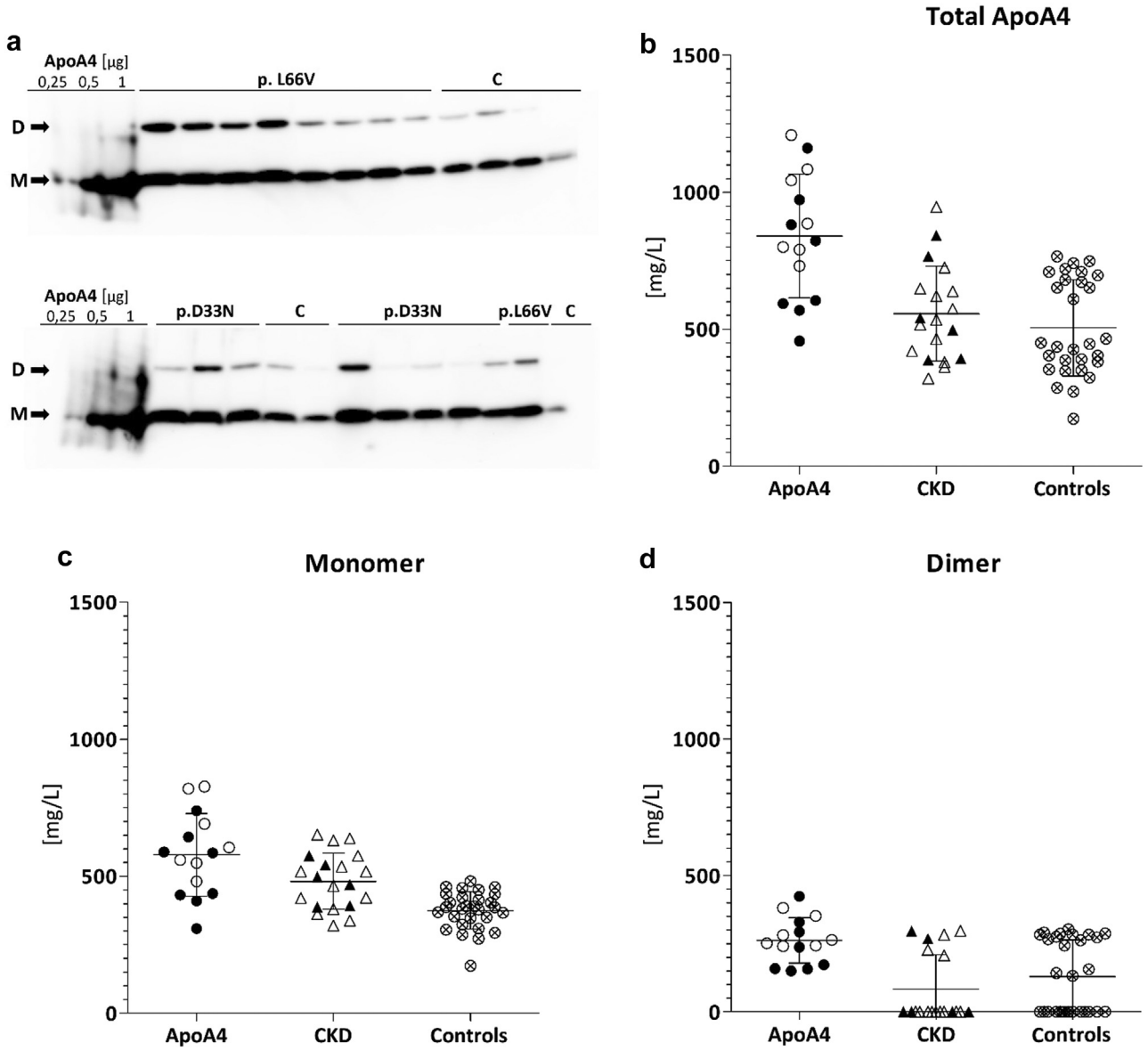

Figure 7 | Plasma ApoA4 concentrations. (**a**) 1 µl of plasma was separated on 3%–25% gradient native polyacrylamide gel electrophoresis polyacrylamide gel; monomeric (M) and dimeric (D) fractions were immunodetected and quantified by densitometry with recombinant ApoA4 as a calibrator. (**b**) The graph represents concentrations of monomer, dimer, and total ApoA4 in genetically affected individuals, individuals with chronic kidney disease (CKD), individuals with *UMOD*, *MUC1*, and *APOA4* mutations, and controls. Black circles indicate individuals with the ApoA4 p.L66V mutation. Unshaded circles indicate individuals with the ApoA4 p.D33N mutation. Black triangles indicate individuals with *MUC1* mutations, and unshaded triangles indicate individuals with *UMOD* mutations. (**b–d**) Plasma levels of total ApoA4 and monomeric ApoA4 were significantly different between individuals with ApoA4 and unaffected individuals (including individuals with *UMOD* and *MUC1* mutations and controls), whereas dimeric levels were not ($P = 0.06$). Plasma levels were not significantly different in comparisons between genetically affected and individuals with *UMOD* or *MUC1* mutations or between genetically affected individuals and controls, likely due to lack of statistical power.

(residues 21–83 and 356–394, respectively; Figure 3a). These terminal domains are involved in transient interactions among themselves and with the central helical domains[28] (Figure 3b), which play a major role in stabilizing ApoA4 tertiary and quaternary structure.

The p.D33N and p.L66V mutations are located at the structurally flexible N-terminal domain (Figure 3c). The altered charge and size of the substituted amino acid residues may disturb the association with other protein domains, such as the C-terminus[29] and may thereby alter protein stability, self-association, and/or lipid binding. Destabilization of the ApoA4 helical structure by amino acid substitutions could also induce formation of alternate secondary structures—including beta-sheets, a basic structural unit of amyloid fibrils (Figure 3d; Supplementary Figure S2).

Two *in silico* prediction programs consistently revealed 2 amyloidogenic regions at the N- and C- terminal domains overlapping at positions of 27–32 and 353–356 (Supplementary Figure S2). Notably, these regions form several contacts in the structural model generated by AlphaFold-Oligomer and may thus form a single amyloidogenic hotspot in the ApoA4 structure. In addition, both pathogenic mutations are near this hotspot. The p.D33N mutation is located in the proximate vicinity, whereas the p.L66V mutation is found in the adjacent interhelical loop. In the analysis of specific mutations, p.D33N caused an expansion of the amyloidogenic region, with both predictive software tools. Similar expansion was found for the p.L66V mutant, using the MetAmyl, but not the AmyloPred2, program.

DISCUSSION

In this investigation, we identified 2 pathogenic variants in *APOA4* as causes of autosomal dominant CKD with a bland urinary sediment in 48 individuals from 5 families. In all, 44 of 47 family members with an eGFR $<$ 60 ml/min per 1.73 m^2 carried an *APOA4* pathogenic variant, and neither variant has been found in the general population. Both variants are evolutionarily conserved and encode for missense mutations in the N-terminal domain relevant to oligomerization of ApoA4.[30] All clinically affected individuals presented with a bland urinary sediment, CKD, and, no clinical evidence of systemic amyloidosis. Routine kidney biopsies limited to the kidney cortex showed tubulointerstitial fibrosis and secondary glomerulosclerosis and no amyloid deposition. Four genetically affected individuals were identified with isolated medullary deposition of amyloid, with mass spectrometry showing the mutated Apoa4 as the primary constituent in 3 available cases.

The majority of filtered ApoA4 likely undergoes intact proximal tubular reabsorption[11] through vesicular transport,[31] similar to albumin.[32] Immunohistochemical studies in normal kidney have demonstrated the presence of ApoA4 in proximal tubular cells, capillaries, blood vessels, and the lymphatic system, but not in glomeruli or distal tubular cells. In proximal tubules, ApoA4 was present in the brush border and in intracellular granules and plasma membranes. ApoA4 was not found in the tubulointerstitium, with no *APOA4* mRNA expression detected in the kidney.[33] These findings are all consistent with reabsorption and degradation of the majority of filtered ApoA4 in proximal tubule cells.

We hypothesize that the amino acid substitutions alter the tertiary or quaternary structure of the mutated ApoA4, leading to increased plasma and primary urine concentrations and isolated medullary amyloid deposition, a finding that is specific to AApoIV amyloidosis—in both sporadic cases[12–14] and patients who have ApoA4 mutations. Pathologic studies performed on the kidney of the proband demonstrated ApoA4-positive amyloid casts in the outer kidney medulla, cortex, and the inner medulla collecting ducts, indicating the ability of ApoA4 to transit the glomerular basement membrane. Abundant ApoA4 staining in the proximal tubule cells indicated increased proximal tubular reabsorption consistent with increased plasma apo4 levels. The mutant ApoA4 is then preferentially deposited in amyloid form in the medulla, possibly because of the increased concentration and due to the medullary gradient and the lower pH environment of the kidney medulla. In fact, the pH of the kidney medulla, approximately 5.5,[34] is very close to the ApoA4 isoelectric point of 5.13,[9] where it denatures and aggregates. Alternatively, N-terminal pathogenic variants may impair intramolecular electron transfer,[35] thus impairing its antioxidant properties[36] and rendering it more vulnerable to free radical attack in the relatively hypoxic environment of the kidney medulla. The deposition of amyloid leads to slowly progressive CKD. As the condition does not primarily affect the glomerulus, the urinary sediment contains no blood or protein.

Identification of pathogenic *APOA4* variants will be clinically challenging for several reasons. Patients present with the mundane clinical findings of slowly progressive CKD with a bland urinary sediment. Given the relatively late onset of kidney disease and the incomplete penetrance in some individuals, the genetic nature of the condition may be missed. In addition, nephrologists may not perform a kidney biopsy due to the slowly progressive nature of the disease and the bland urinary sediment. If a biopsy is performed, it often will include only cortical tissue and result in a nonspecific diagnosis, as occurred in 4 of 6 needle biopsies in this study. Similar to the findings for our proband, Rosenstiel and Alves reported on a patient with sporadic medullary amyloidosis that was found after nephrectomy but not on a prior biopsy.[14] In addition, amyloid deposition was initially missed on 3 of 4 pathologic specimens containing medulla. Thus, diagnosis will rely on a careful family history, *APOA4* sequencing, and ApoA4 immunostaining.

The identification of several genetically affected family members with well-preserved kidney function suggests that environmental or genetic factors may ameliorate the course of disease in this condition. ApoA4 is produced in the intestinal epithelium in response to dietary fat consumption.[7] Reduction in dietary fat content lowers plasma ApoA4 levels,[7] and in the absence of enteral intake, as in patients on total parenteral nutrition, plasma ApoA4 levels fall to nearly undetectable levels.[37] Less ApoA4 production may result in decreased kidney deposition of the mutant protein and could potentially ameliorate kidney disease. We are pursuing investigations in this area. A shortcoming of our study was the small patient population. Given the late onset of disease and its autosomal dominant inheritance, a number of large families have likely suffered from this condition for generations, similar to families with *UMOD*[38–40] and *MUC1* mutations.[41,42] A limitation of this study is the lack of other organ or tissue biopsies to definitively rule out AApoAIV deposition occurring outside of the kidney. Systematic investigations with echocardiography, computed tomography scanning, and ^{123}I-labeled serum amyloid P component (SAP) scintigraphy should be performed in the future to rule out systemic amyloid deposition in these patients.

In summary, we describe 5 families presenting with autosomal dominant medullary amyloidosis due to *APOA4* mutations. ApoA4 is a small protein produced by the small intestine to facilitate fat uptake. Once fat is transported, ApoA4 is filtered by the glomerulus and undergoes tubular reabsorption. Pathogenic *APOA4* variants produce small changes in ApoA4 that do not show clinical signs of affecting lipid transport. However, when mutant ApoA4 is filtered by the glomerulus, the mutation results in fibril formation and amyloid deposition isolated to the kidney medulla, with no clinical evidence of non-kidney deposition. Routine kidney biopsies (which often do not sample the kidney medulla) often show only secondary nephrosclerosis and tubulointerstitial sclerosis but no amyloid deposition. Thus, diagnosis relies on genetic testing. In addition, if medullary amyloidosis is identified in the kidney, formal diagnosis of AApoAIV medullary amyloidosis relies on the identification of the mutated protein either by mass spectrometry, or if the mutation is not known, by the number of spectral counts in the deposits.[12] If the condition is found, patients should undergo genetic analysis of the *APOA4* gene via commercial testing or consultation with an academic center interested in this disorder.

DISCLOSURE

All the authors declared no competing interests.

DATA STATEMENT

Many of the study participants provided consent more than 10 years ago and belonged to very small family units from geographically defined areas with pathogenic variants that are easily identifiable. Given this, the Wake Forest Institutional Review Board did not give permission to share DNA in a repository, due to possible breaches of privacy. However, we can share genetic data from this cohort based on specific data requests, following Wake Forest Institutional Review Board approval of the proposal and a signed data access agreement.

ACKNOWLEDGMENTS

The authors thank all participating patients and families, and the referring physicians. This study was supported by the National Institute for Treatment of Metabolic and Cardiovascular Diseases (CarDia; LX22NPO5104) from the Ministry of Education, Youth and Sports of the Czech Republic, by grants NU21-07-00033 and NV19-08-00137 from the Ministry of Health of the Czech Republic, by the project TN02000132/National Centre for New Methods of Diagnosis, Monitoring, Treatment and Prevention of Genetic Diseases and by institutional programs of Charles University in Prague (UNCE/MED/007 and Cooperation). The National Center for Medical Genomics (LM2023067) kindly provided sequencing and genotyping. CF Structural mass spectrometry of CIISB, Instruct-CZ Centre was supported by MEYS CR (LM2023042), and the European Regional Development Fund-Project "UP CIISB" (No. CZ.02.1.01/0.0/0.0/18_046/0015974) provided proteomic analyses. AJB was funded by the Slim Health Foundation, the Black-Brogan Foundation, and Soli Deo Gloria.

SUPPLEMENTARY MATERIAL

Supplementary File (Word)

Supplementary Figure S1. Additional pedigree branches of Family 3.
Supplementary Figure S2. Amyloidogenic prediction.
Supplementary Figure S3. Urine protein:creatinine ratios for the Wake Forest cohort, and urine albumin:creatinine ratios for the Nova Scotia cohort, according to kidney function and mutation type.
Supplementary Figure S4. Kidney function according to sex. (**A**) Kidney function in affected individuals according to mutation and sex. (**B**) Survival analysis.
Supplementary Figure S5. Light microscopy, including Congo-red staining, of the cortex and medulla in in the nephrectomy specimen from an affected individual.
Supplementary Figure S6. Immunodetection patterns of uromodulin (Tamm–Horsfall protein) and ApoA4 in the kidney cortex and outer kidney medulla of the proband (III.12, Family 1).
Supplementary Figure S7. Control autoptic kidney tissue from an unrelated individual. Immunodetection patterns of uromodulin (Tamm–Horsfall protein) and ApoA4 in the kidney cortex and outer kidney medulla.
Supplementary Figure S8. Plasma Apoa4 immunoaffinity enrichment with mass spectrometry analysis.
Supplementary Methods.
Supplementary Reference.

REFERENCES

1. Zivna M, Kidd KO, Baresova V, et al. Autosomal dominant tubulointerstitial kidney disease: a review. *Am J Med Genet C Semin Med Genet*. 2022;190:309–324.
2. Hart TC, Gorry MC, Hart PS, et al. Mutations of the *UMOD* gene are responsible for medullary cystic kidney disease 2 and familial juvenile hyperuricaemic nephropathy. *J Med Genet*. 2002;39:882–892.
3. Kirby A, Gnirke A, Jaffe DB, et al. Mutations causing medullary cystic kidney disease type 1 lie in a large VNTR in MUC1 missed by massively parallel sequencing. *Nat Genet*. 2013;45:288–393.
4. Groopman EE, Marasa M, Cameron-Christie S, et al. Diagnostic utility of exome sequencing for kidney disease. *N Engl J Med*. 2019;380:142–151.
5. Devuyst O, Olinger E, Weber S, et al. Autosomal dominant tubulointerstitial kidney disease. *Nat Rev Dis Primers*. 2019;5:60.
6. Zivna M, Kidd K, Pristoupilova A, et al. Noninvasive immunohistochemical diagnosis and novel MUC1 mutations causing autosomal dominant tubulointerstitial kidney disease. *J Am Soc Nephrol*. 2018;29:2418–2431.
7. Weinberg RB, Dantzker C, Patton CS. Sensitivity of serum apolipoprotein A-IV levels to changes in dietary fat content. *Gastroenterology*. 1990;98:17–24.
8. Duverger N, Ghalim N, Ailhaud G, et al. Characterization of apoA-IV-containing lipoprotein particles isolated from human plasma and interstitial fluid. *Arterioscler Thromb*. 1993;13:126–132.
9. Weinberg RB, Scanu AM. Isolation and characterization of human apolipoprotein A-IV from lipoprotein-depleted serum. *J Lipid Res*. 1983;24:52–59.
10. Ledford AS, Weinberg RB, Cook VR, et al. Self-association and lipid binding properties of the lipoprotein initiating domain of apolipoprotein B. *J Biol Chem*. 2006;281:8871–8876.
11. Lingenhel A, Lhotta K, Neyer U, et al. Role of the kidney in the metabolism of apolipoprotein A-IV: influence of the type of proteinuria. *J Lipid Res*. 2006;47:2071–2079.
12. Sethi S, Theis JD, Shiller SM, et al. Medullary amyloidosis associated with apolipoprotein A-IV deposition. *Kidney Int*. 2012;81:201–206.
13. Dasari S, Amin MS, Kurtin PJ, et al. Clinical, biopsy, and mass spectrometry characteristics of renal apolipoprotein A-IV amyloidosis. *Kidney Int*. 2016;90:658–664.
14. Rosenstiel PE, Alves T. Diagnosis of AApoAIV medullary amyloidosis at radical nephrectomy. *Kidney Int*. 2022;101:423.
15. Bleyer AJ, Kidd K, Robins V, et al. Outcomes of patient self-referral for the diagnosis of several rare inherited kidney diseases. *Genet Med*. 2020;22:142–149.
16. Hartmannova H, Piherova L, Tauchmannova K, et al. Acadian variant of Fanconi syndrome is caused by mitochondrial respiratory chain complex I deficiency due to a non-coding mutation in complex I assembly factor NDUFAF6. *Hum Mol Genet*. 2016;25:4062–4079.

17. RCSB. Protein data bank. Accessed April 13, 2023. www.rcsb.org/structure/3S84
18. Mirdita M, Schutze K, Moriwaki Y, et al. ColabFold: making protein folding accessible to all. *Nat Methods*. 2022;19:679–682.
19. Emily M, Talvas A, Delamarche C. MetAmyl: a METa-predictor for AMYLoid proteins. *PLoS One*. 2013;8:e79722.
20. Tsolis AC, Papandreou NC, Iconomidou VA, Hamodrakas SJ. A consensus method for the prediction of 'aggregation-prone' peptides in globular proteins. *PLoS One*. 2013;8:e54175.
21. Weinberg RB, Spector MS. Lipoprotein affinity of human apolipoprotein A-IV during cholesterol esterification. *Biochem Biophys Res Commun*. 1986;135:756–763.
22. Dvorak J, Novakova J, Kraftova L, et al. The rapid detection of procalcitonin in septic serum using immunoaffinity MALDI chips. *Clin Proteomics*. 2023;20:20.
23. Levey AS, Stevens LA, Schmid CH, et al. A new equation to estimate glomerular filtration rate. *Ann Intern Med*. 2009;150:604–612.
24. Levine AP, Connor TM, Oygar DD, et al. Combinatorial conflicting homozygosity (CCH) analysis enables the rapid identification of shared genomic regions in the presence of multiple phenocopies. *BMC Genomics*. 2015;16:163.
25. Weinberg RB, Hopkins RA, Jones JB. Purification, isoform characterization, and quantitation of human apolipoprotein A-IV. *Methods Enzymol*. 1996;263:282–296.
26. Weinberg RB. Identification of functional domains in the plasma apolipoproteins by analysis of inter-species sequence variability. *J Lipid Res*. 1994;35:2212–2222.
27. Wen Y, Shah S, Campbell KN. Molecular mechanisms of proteinuria in focal segmental glomerulosclerosis. *Front Med (Lausanne)*. 2018;5:98.
28. Walker RG, Deng X, Melchior JT, et al. The structure of human apolipoprotein A-IV as revealed by stable isotope-assisted cross-linking, molecular dynamics, and small angle x-ray scattering. *J Biol Chem*. 2014;289:5596–5608.
29. Tubb MR, Silva R, Pearson KJ, et al. Modulation of apolipoprotein A-IV lipid binding by an interaction between the N and C termini. *J Biol Chem*. 2007;282:28385–28394.
30. Weinberg RB, Spector MS. The self-association of human apolipoprotein A-IV. Evidence for an in vivo circulating dimeric form. *J Biol Chem*. 1985;260:14279–14286.
31. Russo LM, Sandoval RM, McKee M, et al. The normal kidney filters nephrotic levels of albumin retrieved by proximal tubule cells: retrieval is disrupted in nephrotic states. *Kidney Int*. 2007;71:504–513.
32. Comper WD, Vuchkova J, McCarthy KJ. New insights into proteinuria/albuminuria. *Front Physiol*. 2022;13:991756.
33. Haiman M, Salvenmoser W, Scheiber K, et al. Immunohistochemical localization of apolipoprotein A-IV in human kidney tissue. *Kidney Int*. 2005;68:1130–1136.
34. Zalyapin EA, Bouley R, Hasler U, et al. Effects of the renal medullary pH and ionic environment on vasopressin binding and signaling. *Kidney Int*. 2008;74:1557–1567.
35. Weinberg RB. Exposure and electronic interaction of tyrosine and tryptophan residues in human apolipoprotein A-IV. *Biochemistry*. 1988;27:1515–1521.
36. Wong WM, Gerry AB, Putt W, et al. Common variants of apolipoprotein A-IV differ in their ability to inhibit low density lipoprotein oxidation. *Atherosclerosis*. 2007;192:266–274.
37. Weinberg RB, Sherman JR. Serum apolipoprotein A-IV and lipoprotein cholesterol in patients undergoing total parenteral nutrition. *Gastroenterology*. 1988;95:394–401.
38. Valluru MK, Chung NK, Gilchrist M, et al. A founder UMOD variant is a common cause of hereditary nephropathy in the British population. *J Med Genet*. 2023;60:397–405.
39. Smith GD, Robinson C, Stewart AP, et al. Characterization of a recurrent in-frame UMOD indel mutation causing late-onset autosomal dominant end-stage renal failure. *Clin J Am Soc Nephrol*. 2011;6:2766–2774.
40. Bleyer AJ, Woodard AS, Shihabi Z, et al. Clinical characterization of a family with a mutation in the uromodulin (Tamm-Horsfall glycoprotein) gene. *Kidney Int*. 2003;64:36–42.
41. Stavrou C, Pierides A, Zouvani I, et al. Medullary cystic kidney disease with hyperuricemia and gout in a large cypriot family: no allelism with nephronophthisis type 1. *Am j Med Genet*. 1998;77:149–154.
42. Kiser RL, Wolf MTF, Martin JL, et al. Medullary cystic kidney disease type 1 in a large Native-American kindred. *Am J Kidney Dis*. 2004;44:611–617.